Simulation of Hydrosol Deposition in Granular Media

Chang-upp Choo and Chi Tien
Dept. of Chemical Engineering and Materials Science, Syracuse University, Syracuse, NY 13244

An algorithm is developed for simulating particle deposition from liquid suspensions flowing through granular media, specifically the prediction of the extent of deposition and the change of media permeability on a local basis. The formulation is based on the premise that granular media may be considered as an assembly of collectors represented by a dual-configuration—either spherical or capillaric—to be applied for deposition and permeability reduction considerations. Comparisons with experiments indicate that the simulation algorithm can indeed be used as a predictive tool for estimating the transport and distribution of particulate matter in granular media.

Introduction

The problems arising from the deposition of particles from suspensions flowing through granular media are of importance to a number of engineering and natural systems. For example, proper design of deep-bed filters for water and waste water treatment requires the knowledge of particle deposition rates. Similarly, information concerning the degree of media clogging and the accompanying increase in hydraulic resistance is crucial in considering water injection for oil recovery from reservoirs. It is also apparent that a predictive capability concerning the distribution and transport of particles in ground-water flow cannot be developed without a quantitative understanding of these problems.

We can consider particle deposition in granular media as follows: As a suspension flows through a granular medium, some of the suspended particles may be transported to and come into contact with the surface of the medium matrix. If the surface interactions are favorable, these particles may become deposited. At the same time, particle deposition alters the medium's structure and/or the nature of the surface interactions. The change of the medium structure implies a change of medium permeability or its hydraulic resistance. Similarly, a change in the surface interactions and/or that of media permeability may affect particle deposition rates. Since these changes occur continuously, the physical process is inherently a nonsteady state. In other words, the extent of deposition, medium permeability, and suspension particle concentration are local, time-dependent functions.

Present address of C.-u. Choo: Samsung Engineering Co. Ltd., R&D Center, Yongin-Koon Kyunggi-Do, Korea 449-510.
Present address of C. Tien: Dept. of Chemical Engineering, National University of Singapore, Singapore 0511.

Because of their practical importance, several aspects of the deposition and flow problems have attracted the attention of a number of investigators. Studies on deposition rates in media free of deposition were made by Yao et al. (1971), Spielman and FitzPatrick (1973), Payatakes et al. (1974), Rajagopalan and Tien (1976, 1977), and others by applying the trajectory analysis. The effect of the surface interaction was examined by Vaidyanathan and Tien (1988, 1991). Since the extent of deposition was assumed negligible in these studies, the transient-state behavior was not considered.

For a more complete description of deep-bed filtration, several empirical models have been proposed in the past. (For a summary of these works, see Tien, 1989.) Several rational models have appeared in the literature (O'Melia and Ali, 1978; Tien et al., 1979; Chiang and Tien, 1985a; Vigneswaran and Tien, 1987; Mackie et al., 1987; Vigneswaran and Tulachan, 1988). All of these models were concerned with filter performance during the so-called "ripening period." While all the models are able to give reasonable predictions of effluent concentration histories, these models do not address the problem of media clogging and permeability reductions.

The fact that porous media models based on simple geometry fail to account for permeability reduction due to deposition is not surprising. To explain the changes in media permeability, one must consider not only the presence of deposits on the filter grains (or the change in individual pore space), but also the effect of deposition on the distribution of fluid flow through the pore space of the medium. As the extent of deposition increases, a given pore may become blocked and not available to flow. This feature must be incorporated

into the model if the model is to correctly predict the permeability changes due to deposition.

The model that has often been used in characterizing porous medium permeability is the network model proposed by Fatt (1956). The model represents a porous medium by a collection of nodes connecting to each other by bonds. By specifying the sizes and size distributions of these nodes and bonds and the manner with which the neighboring nodes are connected and by specifying the geometries of these entities, a network model can be constructed to represent certain static and dynamic properties of porous media. More recently several investigators have used the network model in describing the flow of suspensions through porous media (Rege and Fogler, 1987, 1988; Imdakm and Sahimi, 1987, 1991)

There are two major problems in applying the network model for deposition studies. First, with a large number of nodes, an excessive amount of computation is required. Second, the capillaric geometry is not suitable for estimating particle collection (Payatakes et al., 1974) except for collection by straining. For this reason, in studies involving the use of the network model, deposition is often limited to relatively large particles (as compared with void space).

In the present work, we propose a new model for simulating the deposition of particles from suspensions flowing through granular media and particularly in predicting the extent of deposition and the reduction in media permeability. The model assumes a medium to be an assembly of spheres or capillaries of different sizes. This dual representation makes it possible to consider the interactions between deposition and permeability reduction without excessive computations.

Model Description

Consider the flow of a suspension through a granular medium. The medium may be considered to be a number of unit bed elements of length l connected in series (see Figure 1). Each unit bed element is composed of M unit collectors. According to Payatakes et al. (1974), l is given as

$$l = \left[\frac{\pi}{6(1-\epsilon_0)}\right]^{1/2} d_g \tag{1}$$

where d_g is the grain diameter and ϵ_0 the initial medium porosity. Thus for a medium of height L, the number of unit-bed elements involved, N, is

$$N = L/l. \tag{2}$$

For a given unit-bed element, the entering suspension is distributed over the M unit collector according to their hydraulic conductivities. The effluents from these M collectors are thoroughly mixed to form the influent to the next unit-bed element. The effluent concentration is determined by deposition taking place in all the unit collectors. Similarly, the permeability of the medium is determined from the hydraulic conductivities of these collectors.

Determining the hydraulic conductivity of a collector requires the specification of its geometry. For this reason, the collectors are assumed to be capillaries of various sizes. With

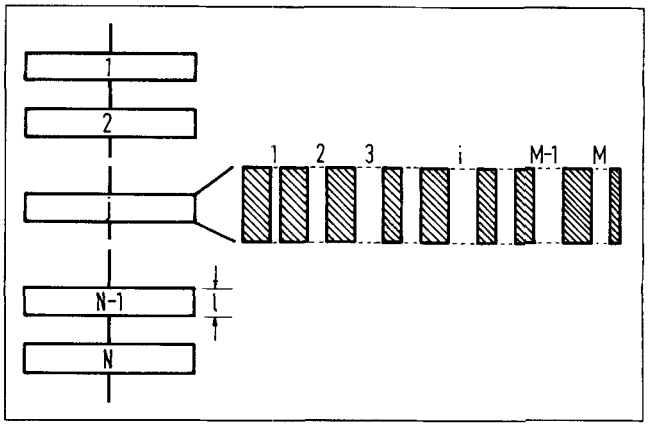

Figure 1. Unit-bed-element model proposed in this study.

the suspension flowing through and deposition taking place in these collectors, the collector geometries change accordingly. Since the collector efficiency expression is based on a spherical geometry, an equivalent criterion between a spherical and a capillaric collector has to be developed.

In the following section, we present the method used for determining the initial collector sizes, particle deposition rates of the collectors, and the corresponding changes in capillary geometry and the hydraulic conductances of the collectors.

Specification of capillary sizes

To specify the capillary sizes of a unit-bed element, the results of Payatakes (1973) are applied. Based on the constricted-tube model (see Figure 2), Payatakes proposed a procedure for determining the pore constriction distribution from capillary pressure-saturation data. Accordingly, if one assumes that a constricted tube can be approximated by a capillary, the capillary size distribution can be readily obtained from the pore constriction distribution data.

The conversion of constricted tubes to capillaries is based on the pore volume equivalence. The geometry of a constricted tube of Payatakes is determined by its height, h_i, maximum diameter, a_i, and constriction diameter, d_i, with

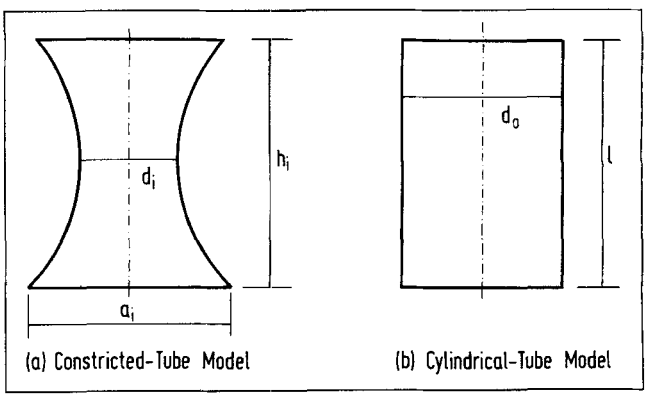

Figure 2. Unit cells of the *i*th type of the constricted tube and its corresponding cylindrical tube.

(a) Constricted-tube model. (b) Cylindrical-tube model.

a_i/h_i, and d_i/h_i being constant. The volume of a constricted tube of the ith type, $(V_{pe})_i$, can be expressed as

$$(V_{pe})_i = c_0 c_1 (d_i)^3 \tag{3}$$

where $c_0 = \pi/6$,

$$c_1 = \left[\frac{\epsilon_0(1-S_{wi})}{1-\epsilon_0} \frac{< d_g^3 >}{< d_c^3 >} \right]^{1/3},$$

and S_{wi} is the irreducible saturation; also $< d_g >$ and $< d_c >$ are the effective grain diameter and constriction diameter, respectively. By equating the volume of a cylindrical pore of diameter $(d_0)_i$ and length l to the volume of a constricted tube of Payatakes, one has

$$(d_0)_i = \sqrt{\frac{4c_0c_1}{\pi l}(d_i)^3}. \tag{4}$$

Equation 4 can be used to convert the pore constriction distribution data into the necessary capillary size distribution.

Calculation of Media Permeability

The method that can be used to estimate the change in the local medium permeability as a function of the extent of deposition (expressed as the number of deposited particles per capillary) is as follows. Consider there are N_c pores of various sizes in a unit cross-sectional area of a unit-bed element (UBE). The fluid flow through a single pore of the ith type is given as

$$q_{ij} = \alpha_{ij}(P_{j-1} - P_j) \tag{5}$$

where the subscripts i and j denote the ith pore and jth UBE, respectively; q_{ij} and α_{ij} are the volumetric flow rate and the conductivity of the ith pore in the jth UBE; and P_{j-1} and P_j are the upstream pressure and the downstream pressure of the jth UBE.

By definition, the superficial velocity of a filter bed, μ_s, is

$$u_s = \sum_{i=1}^{N_c} q_{ij} = (Q_T)_j \tag{6}$$

where $(Q_T)_j$ is total flow rate through the jth UBE.

The hydraulic conductivity of the jth UBE, α_j, is expressed as

$$\alpha_j = \sum_{i=1}^{N_c} \alpha_{ij}. \tag{7}$$

Then the distribution of fluid flow in the jth UBE is obtained by

$$\frac{q_{ij}}{(Q_T)_j} = \frac{\alpha_{ij}}{\alpha_j}, \tag{8}$$

and the change in permeability of the jth UBE due to deposition may be expressed as

$$\frac{(K_j)}{(K_j)_0} = \frac{(\alpha_j)}{(\alpha_j)_0}. \tag{9}$$

For constant throughput operation, one has

$$\frac{(P_{j-1}-P_j)}{(P_{j-1}-P_j)_0} = \frac{(\Delta P_j)}{(\Delta P_j)_0} = \frac{(\alpha_j)}{(\alpha_j)_0} = \frac{(K_j)_0}{(K_j)} \tag{10}$$

where ΔP_j denotes the pressure drop across the jth UBE and the subscript 0 has the same meaning as before.

For a medium with N unit-bed elements connected in series, the ratio of the pressure drop across the medium to its initial value becomes

$$\frac{\Delta P}{(\Delta P)_0} = \frac{\sum_{j=1}^{N}(\Delta P_j)}{\sum_{j=1}^{N}(\Delta P_j)_0} = \frac{\sum_{j=1}^{N} 1/(\alpha_j)}{\sum_{j=1}^{N} 1/(\alpha_j)_0} = \frac{\sum_{j=1}^{N} 1/(K_j)}{\sum_{j=1}^{N} 1/(K_j)_0} = \frac{1/K}{1/K_0} \tag{11}$$

where K is the average permeability of the medium over a length of L (corresponding to N unit-bed elements).

To assess the effect of pore plugging and estimate the permeability reduction, it is necessary to take into account the deposit morphology. If a nonuniform layer of deposit is formed over the pore surface, the effective radius of the capillary can be assumed to be

$$R_{ij} = (R_d)_{ij} + \{(R_0)_{ij} - (R_d)_{ij}\}\left(\frac{z}{l}\right)^n \tag{12a}$$

or

$$\frac{R_{ij}}{(R_0)_{ij}} = \frac{(R_d)_{ij}}{(R_0)_{ij}} + \left\{1 - \frac{(R_d)_{ij}}{(R_0)_{ij}}\right\}\left(\frac{z}{l}\right)^n \tag{12b}$$

where R_{ij} is the local radius of the ith pore in the jth UBE; $(R_d)_{ij}$ is the value of R_{ij} at the inlet of the cylindrical pore; n is a constant and is assumed to be the same for capillaries of all sizes; and z is the capillary axial distance measured from the inlet. If the number of deposited particles in a capillary is $(N_p)_{ij}$, $(R_d)_{ij}$ can be determined from

$$(R_d)_{ij} = \frac{-(R_0)_{ij} + \sqrt{(R_0)_{ij}^2 - 4n\left\{\frac{(N_p)_{ij}}{6(1-\epsilon_d)}\frac{(2n+1)(n+1)}{2nl}d_p^3 - (R_0)_{ij}^2(n+1)\right\}}}{2n}. \tag{13}$$

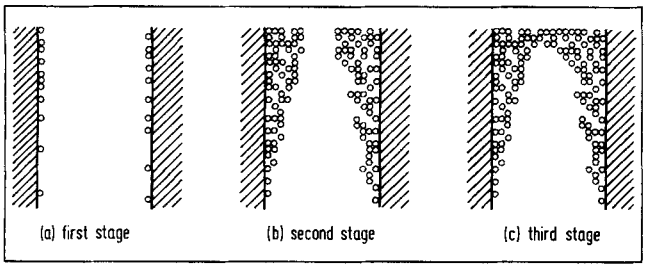

Figure 3. Three stages of particle deposition.
(a) First stage. (b) Second stage. (c) Third stage.

The choice of n in Eq. (12a) is somewhat arbitrary; it may be chosen to give the best fit with experimental data in permeability reduction. Also, one can expect that n depends on the ratio of particle diameter to grain diameter, N_R. With small N_R, the distribution of particle deposit tends to be more uniform leading to a larger value of n. On the other hand, with large N_R, particles will be deposited mostly near the pore inlet leading to a more nonuniform deposition and a smaller value of n.

To estimate permeability reduction due to deposition, we consider the fact that deposition proceeds in three stages (Figure 3): During the first stage, particles are deposited individually on the pore surface. The first stage terminates when sufficient particles are deposited to form a layer of a thickness equal to that of one particle diameter [or the value of $(R_0)_{ij}-(R_d)_{ij}$ of Eq. 13 is equal to d_p]. During the second stage, particle deposition results in the formation of a multilayer particle deposit. The second stage ceases when $(R_d)_{ij}$ becomes sufficiently small such that sieving (straining) becomes the dominant mechanism of deposition. The third stage of deposition is assumed to begin when $(R_d)_{ij}$ is equal to a certain multiple of the particle radius (i.e., either three or seven). This assumption is similar to the third on seventh rule of Todd et al. (1984). The exact value to be used can be determined by comparing predictions with experiments to be explained later. The result of the third stage of deposition is the formation of a deposit layer at the inlet (or the so-called internal cake). The occurrence of the third-stage deposition depends upon the magnitude of the interstitial fluid velocity. With high fluid velocity, particle deposition may become impossible. This point will be discussed further in later sections.

First stage of particle deposition

The initial conductivity of a cylindrical pore, $(\alpha_{ij})_0$ (see Eq. 5), according to the Hagen-Poiseuille equation, is given as

$$(\alpha_{ij})_0 = \frac{\pi d_{ij}^4}{128\mu l} \tag{14}$$

where d_{ij} and l are diameter and length of the ith capillary in the jth UBE.

When a particle becomes deposited on the surface of a cylindrical pore, as shown in Figure 4, the increase of the resistance to fluid flow may be obtained from the drag force experienced by the deposited particle. The pressure drop, ΔP_p, due to one deposited particle can be approximated as (Happel and Brenner, 1973)

$$\Delta P_p = \frac{12\mu a_p U_0}{R_0^2}\left\{1-\left(1-\frac{a_p}{R_0}\right)^2\right\}^2 K_1 \tag{15}$$

and

$$K_1 = \frac{1-\frac{2}{3}\left(\frac{a_p}{R_0}\right)^2-0.20217\left(\frac{a_p}{R_0}\right)^5}{1-2.1050\left(\frac{a_p}{R_0}\right)+2.0865\left(\frac{a_p}{R_0}\right)^3-1.7068\left(\frac{a_p}{R_0}\right)^5+0.72603\left(\frac{a_p}{R_0}\right)^6} \tag{16}$$

where U_0 is the center-line velocity of the pore; a_p and R_0 are the particle and pore radii, respectively. The total pressure drop, ΔP_{total}, across the pore is

$$\Delta P_{\text{total}} = \Delta P_{\text{tube}} + \Delta P_p \tag{17}$$

where ΔP_{tube} is the pressure drop of the clean tube. If the number of deposited particles is $(N_p)_{ij}$ and if there are no interactions between deposited particles, α_{ij} is given as

$$\frac{1}{\alpha_{ij}} = \frac{1}{(\alpha_{ij})_0}+\frac{1}{\alpha_p} = \frac{8\mu l}{\pi R_0^4}+\frac{24\mu (N_p)_{ij}}{\pi R_0^4}a_p\left\{1-\left(1-\frac{a_p}{R_0}\right)^2\right\}^2 K_1. \tag{18}$$

The preceding expression applies if $(R_0)_{ij}-(R_d)_{ij} < d_p$.

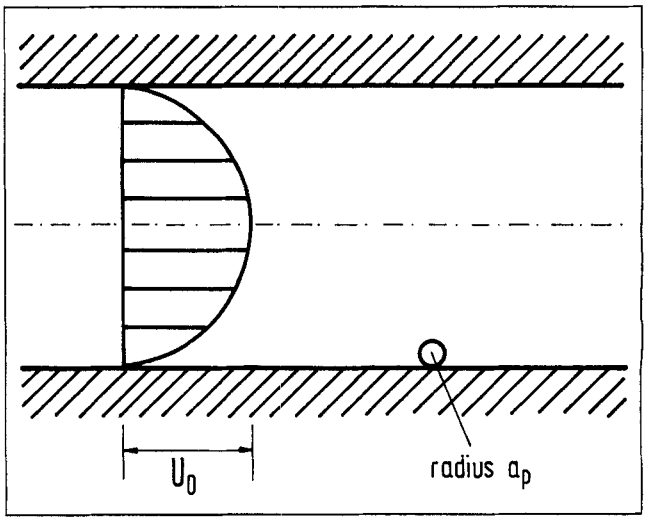

Figure 4. Deposited particle and fluid motion inside a cylindrical pore.

Second stage of particle deposition

With a multilayer deposit, a capillary can be divided into MN segments of equal length (Figure 5). The deposit in each segment is considered uniform. For each segment, if one assumes the Hagen-Poiseuille flow within the empty pore space and the Brinkman flow in the deposit layer, then the flow field within one segment can be found from the solution of the following equations:

(a) For the empty pore space, or region A $(0 < r < R_c)$

$$\frac{\mu}{r}\frac{d}{dr}\left(r\frac{dv_z^A}{dr}\right)=\frac{dP}{dz}. \tag{19}$$

(b) For the deposit layer, or region B $(R_c < r < R_0)$

$$\frac{\mu}{r}\frac{d}{dr}\left(r\frac{dv_z^B}{dr}\right)-\frac{\mu}{k_d}v_z^B=\frac{dP}{dz}. \tag{20}$$

The boundary conditions are

$$\begin{aligned} &v_z^A = \text{finite} && && \text{at } r=0\\ &v_z^A = v_z^B, && \tau_{rz}^A=\tau_{rz}^B && \text{at } r=R_c\\ &v_z^A = 0 && && \text{at } r=R_0 \end{aligned} \tag{21}$$

where the superscripts A and B refer to regions A and B, respectively; v_z is fluid velocity along the axial direction and τ_{rz}, the shear stress; and μ is the fluid velocity. The value of R_c is taken as the average value from the deposit profile in each segment according to Eq. 12a (Figure 5). For the kth segment, R_c is given as

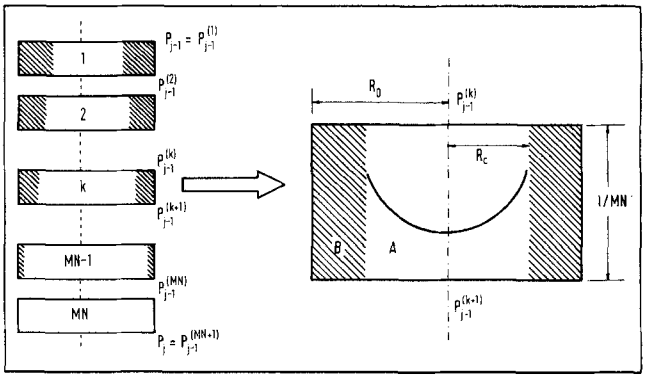

Figure 5. Flow field description inside a cylindrical pore.

$$C_1^B=\frac{k_dK_1\left(\frac{R_c}{\sqrt{k_d}}\right)+\frac{R_c}{2}\sqrt{k_d}K_0\left(\frac{R_0}{\sqrt{k_d}}\right)}{I_0\left(\frac{R_0}{\sqrt{k_d}}\right)K_1\left(\frac{R_c}{\sqrt{k_d}}\right)+I_1\left(\frac{R_c}{\sqrt{k_d}}\right)K_0\left(\frac{R_0}{\sqrt{k_d}}\right)} \tag{25a}$$

$$C_2^B=\frac{k_dI_1\left(\frac{R_c}{\sqrt{k_d}}\right)-\frac{R_c}{2}\sqrt{k_d}I_0\left(\frac{R_0}{\sqrt{k_d}}\right)}{I_0\left(\frac{R_0}{\sqrt{k_d}}\right)K_1\left(\frac{R_c}{\sqrt{k_d}}\right)+I_1\left(\frac{R_c}{\sqrt{k_d}}\right)K_0\left(\frac{R_0}{\sqrt{k_d}}\right)} \tag{25b}$$

$$C_1^A=-\frac{R_c^2}{4}-k_d+C_1^BI_0\left(\frac{R_c}{\sqrt{k_d}}\right)+C_2^BK_0\left(\frac{R_c}{\sqrt{k_d}}\right) \tag{25c}$$

and I_n and K_n are the modified Bessel functions of the first kind and the second kind of order n; and $P_{j-1}^{(k)}$ and $P_{j-1}^{(k+1)}$ denote the upstream and the downstream pressures of the kth segment in the jth UBE.

$$R_c=\sqrt{(R_d)_{ij}^2+\frac{2(R_d)_{ij}\{(R_0)_{ij}-(R_d)_{ij}\}}{n+1}\frac{k^{n+1}-(k-1)^{n+1}}{(MN)^n}+\frac{\{(R_0)_{ij}-(R_d)_{ij}\}^2}{2n+1}\frac{k^{2n+1}-(k-1)^{2n+1}}{(MN)^{2n}}}. \tag{22}$$

The solutions of Eqs. 19 and 20 with the boundary conditions of Eq. 21 give the velocity profiles within regions A and B:

$$v_z^A=\frac{P_{j-1}^{(k+1)}-P_{j-1}^{(k)}}{\mu(l/MN)}\left(\frac{r^2}{4}+C_1^A\right) \tag{23}$$

$$v_z^B=\frac{P_{j-1}^{(k+1)}-P_{j-1}^{(k)}}{\mu(l/MN)}\left\{-k_d+C_1^BI_0\left(\frac{r}{\sqrt{k_d}}\right)+C_2^BK_0\left(\frac{r}{\sqrt{k_d}}\right)\right\} \tag{24}$$

where

The total flow rate is determined by

$$\begin{aligned} Q&=\int_0^{R_c}v_z^A2\pi r\,dr+\int_{R_c}^{R_0}v_z^B2\pi r\,dr\\ &=2\pi\frac{P_{j-1}^{(k+1)}-P_{j-1}^{(k)}}{\mu(1/MN)}\left[\left(\frac{R_c^4}{16}+C_1^A\frac{R_c^2}{2}\right)+\left\{\frac{k_d(R_c^2-R_0^2)}{2}\right.\right.\\ &\quad+C_1^B\sqrt{k_d}\left(R_0I_1\left(\frac{R_0}{\sqrt{k_d}}\right)-R_cI_1\left(\frac{R_c}{\sqrt{k_d}}\right)\right)\\ &\quad\left.\left.+C_2^B\sqrt{k_d}\left(R_cK_1\left(\frac{R_c}{\sqrt{k_d}}\right)-R_0K_1\left(\frac{R_0}{\sqrt{k_d}}\right)\right)\right\}\right]. \end{aligned} \tag{26}$$

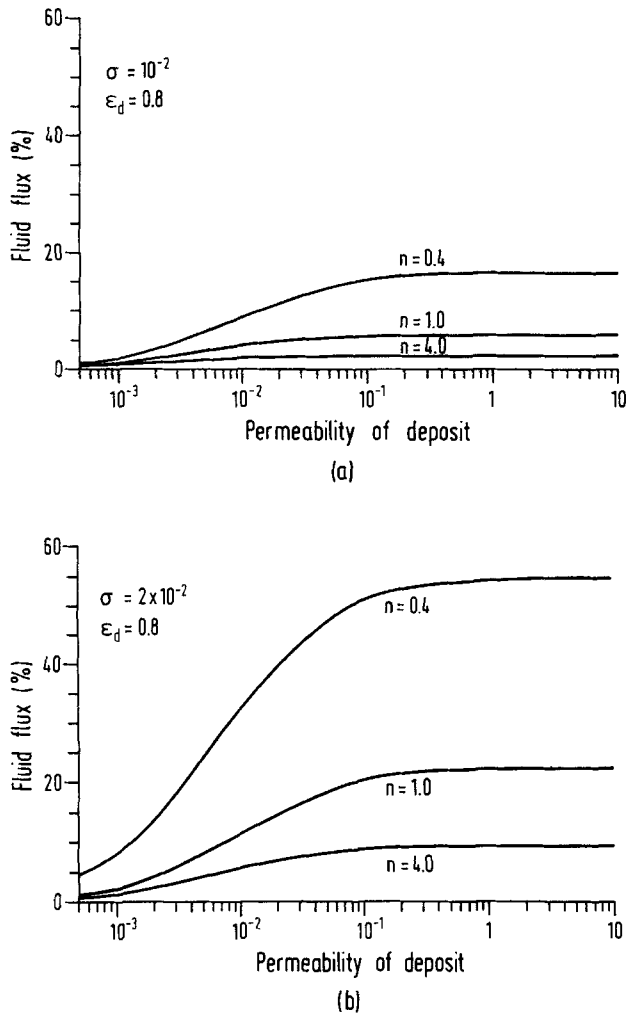

Figure 6. Fraction of fluid flow through the deposit layer in the first segment of a cylindrical pore shown in Figure 5.

From Eq. 26, the conductivity of the kth segment, $\alpha_{ij}^{(k)}$, is

$$\alpha_{ij}^{(k)} = \frac{-2\pi}{\mu(1/MN)}\left[\left(\frac{R_c^4}{16} + C_1^A\frac{R_c^2}{2}\right) + \left\{\frac{k_d(R_c^2 - R_0^2)}{2} + C_1^B\sqrt{k_d}\left(R_0 I_1\left(\frac{R_0}{\sqrt{k_d}}\right) - R_c I_1\left(\frac{R_c}{\sqrt{k_d}}\right)\right) + C_2^B\sqrt{k_d}\left(R_c K_1\left(\frac{R_c}{\sqrt{k_d}}\right) - R_0 K_1\left(\frac{R_0}{\sqrt{k_d}}\right)\right)\right\}\right] \quad (27)$$

Since these segments are connected in series to form a cylindrical pore, the conductivity of the cylindrical pore can be expressed as

$$\frac{1}{\alpha_{ij}} = \sum_{k=1}^{MN}\frac{1}{\alpha_{ij}^{(k)}}. \quad (28)$$

Figure 6 shows the fraction of the fluid flow through the deposit layer of the first segment of a capillary. One can see that the permeability of the deposit layer has a significant effect on the flow through the deposit layer and on permeability reduction.

Third stage of particle deposition

During this stage, capillaries can become blocked by deposited particles. With $(R_d)_{ij}$ (see Eq. 13) reaching certain critical values (i.e., three or seven times particle radius), particle deposition leads to the formation of particle deposit layers at the inlet of the capillaries with porosity of ϵ_{d_2} (Figure 7). The pore conductivity becomes

$$\frac{1}{(\alpha_{ij})_T} = \frac{1}{\alpha_{ij}} + \frac{1}{(\alpha_{ij})_{\text{plug}}} \quad (29)$$

where $(\alpha_{ij})_T$ is the overall conductivity of the pore, and α_{ij} is the pore conductivity at the end of the second stage of deposition and is given by Eq. 28; and $(\alpha_{ij})_{\text{plug}}$ is the conductivity of the filter cake formed at the inlet and is given as

$$(\alpha_{ij})_{\text{plug}} = \frac{-2\pi}{\mu l_d}\left\{-\frac{k_{d_2}R_0^2}{2} + C_1^B\sqrt{k_{d_2}}R_0 I_1\left(\frac{R_0}{\sqrt{k_{d_2}}}\right) - C_2^B\sqrt{k_{d_2}}R_0 K_1\left(\frac{R_0}{\sqrt{k_{d_2}}}\right)\right\}. \quad (30)$$

Note that the preceding expression is obtained from Eq. 27 with $R_c = 0$ and k_{d_2} and l_d in place of k_d and l/MN, where l_d and k_{d_2} are the thickness and permeability of the cake.

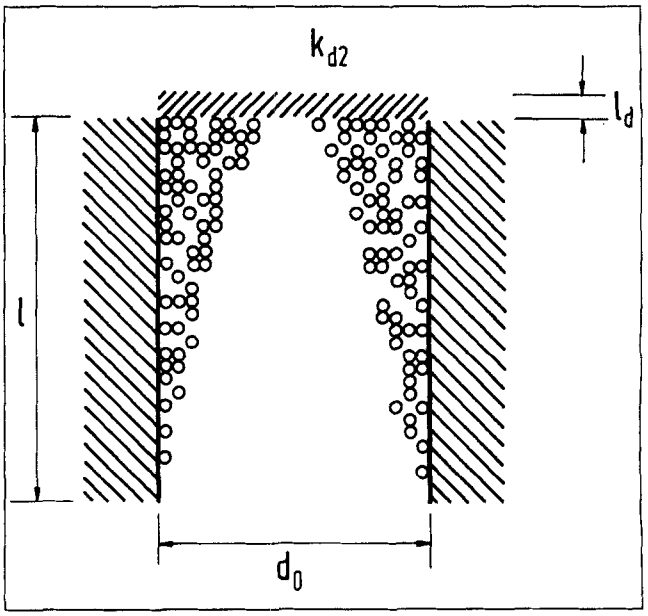

Figure 7. Assumed particle deposit shape during the third stage of particle deposition process.

Estimation of Capillary Collection Efficiencies

As shown in the preceding section, predicting permeability reduction requires the knowledge of the particle deposition taking place in each and every capillary present in a UBE. Collection efficiencies predicted on the basis of the capillaric geometry have not yielded satisfactory results (Payatakes et al., 1974). On the other hand, reasonably accurate expressions for the initial collection efficiency and the change in collection efficiency due to deposition based on the sphere-in-cell models are available (Rajagopalan and Tien, 1976; Chiang and Tien, 1985b; Choo, 1993). In the following we outline a procedure by which collection efficiencies of the individual capillaries may be estimated from information based on the spherical geometry.

Initial collection efficiency

If one assumes that all the unit cells within a UBE are identical spheres, then the number of cells in a UBE of unit cross-sectional area is given as

$$N_H = \left[\frac{6(1-\epsilon_0)}{\pi}\right]^{2/3} (d_g)^{-2} \tag{31}$$

where N_H is the number of unit cells in a UBE of unit cross-sectional area.

The initial collection efficiency of the unit cells can be estimated from the expression developed by Rajagopalan and Tien (1976), or

$$\eta_{H_0} = 1.5A_s(1-\epsilon_0)^{2/3}N_R^2\left\{\frac{2}{3}N_{Lo}^{1/8}N_R^{-1/8} + 2.25 \times 10^{-3}N_G^{1.2}N_R^{-2.4}\right\} + 4(1-\epsilon_0)^{2/3}A_s^{1/3}N_{Pe}^{-2/3} \tag{32}$$

where η_{H_0} is the initial collection efficiency of the unit cell (Happel's cell); N_{Lon}, N_R, N_{Pe}, and A_s are the London force parameter, gravitational parameter, interception parameter, Peclet number, and Happel's parameter (see Notation for their definitions), respectively. The relationship between the collection efficiency of a UBE and that of a Happel's cell is (Tien, 1989),

$$\eta_{u_0} = 1.209\eta_{H_0} \tag{33}$$

where η_{u_0} is the initial collection efficiency of the UBE.

To apply the results of Eq. 32 to individual capillaries, the initial collection efficiency of the UBE can be expressed as

$$\eta_{u_0} = \frac{1}{Q_T}(q_{10}\eta_{1_0} + q_{20}\eta_{2_0} + \cdots + q_{N_c0}\eta_{N_{c0}}) \tag{34}$$

where Q_T is the total flow rate through the UBE expressed as

$$Q_T = \sum_{i=1}^{N_c} q_{i_0} = \sum_{i=1}^{N_c} q_i \tag{35}$$

and q_{i_0} and η_{i_0} are the initial flow rate and the initial collection efficiency of the ith capillary of the UBE.

To obtain the initial collection efficiency of the ith capillary, according to Rajagopalan and Tien (1976), the initial collection efficiency due to interception based on Happel's model, η_I, is

$$\eta_I = 1.5A_s(1-\epsilon_0)N_R^2. \tag{36}$$

On the basis that interception is dominant deposition mechanism, the initial collection efficiency of the ith capillary may be assumed to be proportional to the square of the ratio of the particle diameter, d_p, to the pore diameter, $(d_0)_i$, or

$$\eta_{i_0} = C_p\left\{\frac{d_p}{(d_0)_i}\right\}^2 \tag{37}$$

where C_p is a proportionality constant and is taken to be constant for capillaries of all sizes. Substituting Eq. 37 into Eq. 34, C_p is found to be

$$C_p = \frac{Q_T\eta_{u_0}}{\sum_{i=1}^{N_c} q_{i_0}\left\{\frac{d_p}{(d_0)_i}\right\}^2}. \tag{38}$$

With the initial collection efficiency of the UBE, η_{u_0}, determined from Eqs. 32 and 33, the initial collection efficiency of the ith capillary can then be estimated from Eqs. 37 and 38.

Collection efficiencies during the first and second stages of particle deposition

During the first and second stages of deposition, the rate of deposition can be expected to increase with the increase of the extent of deposition. In the terminology of deep-bed filtration, this period is known as the ripening period. An expression that gives the increases in the unit collector efficiency during this period has been recently obtained by Choo (1993) and is given as

$$\frac{\eta_H}{\eta_{H_0}} = Y\left\{1 + 9.61(1-\epsilon_0)^{2/3}\left(\frac{\sigma}{1-\epsilon_d}\right)\right\} + (1-Y)\left\{1 + \frac{0.6794}{1-\epsilon_0}\left(\frac{1}{N_R} - 0.921\right)\left(\frac{\sigma}{1-\epsilon_d}\right) + \frac{0.1731}{(1-\epsilon_0)^2}\left(\frac{1}{N_R^2} + \frac{3}{N_R} - 1.171\times 10^2\right)\left(\frac{\sigma}{1-\epsilon_d}\right)^2\right\} \tag{39}$$

where

$$Y=\frac{0.598k_d^{-0.8}\left(1+\dfrac{0.0128}{N_R}\right)\left\{\dfrac{\sigma}{5(1-\epsilon_d)}\right\}^{(1.63+5.5\times10^{-4}/N_R)}\left(\dfrac{1}{1-\epsilon_0}\right)^2}{1+0.598k_d^{-0.8}\left(1+\dfrac{0.0128}{N_R}\right)\left\{\dfrac{\sigma}{5(1-\epsilon_d)}\right\}^{(1.63+5.5\times10^{-4}/N_R)}\left(\dfrac{1}{1-\epsilon_0}\right)^2}. \quad (40)$$

According to Eq. 39, η_H/η_{H_0} in Figure 8a is shown as a function of the specific deposit for three different values of N_R with $\epsilon_d = 0.8$ and $\epsilon_0 = 0.4$ (values that correspond to typical conditions of granular media in filtration). The results shown in Figure 8a may also be presented in the form of the collection efficiency ratio vs. the number of deposited particles (see Figure 8b). It is clear that over a range of the specific deposit values (i.e., $0 < \sigma < 8\times10^{-3}$), the relationship shown in Figure 8b is largely linear, or

$$\frac{\eta_H}{\eta_{H_0}} = 1 + B^*(\text{No. of deposited particles}). \quad (41)$$

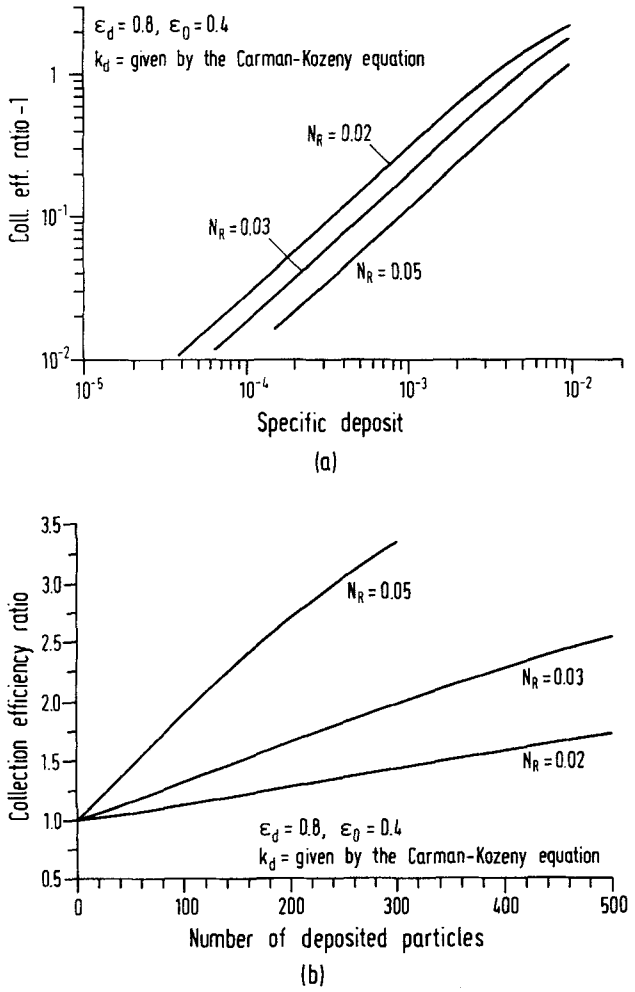

Figure 8. Collection efficiency vs. specific deposit and the number of deposited particles according to Eq. 39.

The value of B is simply

$$B = \frac{\left(\dfrac{\eta_H}{\eta_{H_0}} - 1\right)}{\text{No. of deposited particles}} \quad (42)$$

where B represents the increase in collection efficiency per deposited particle. Since the simulation scheme gives the number of particles deposited for each capillary as a function of time, Eq. 41 provides a convenient way of estimating the change in collection efficiency due to deposition.

Consider a UBE with unit cross-sectional area and with N_H Happel's cells. With the deposition of one particle in one of the N_H cells, the collection efficiency of the UBE, η_{u_1}, is

$$\eta_{u_1} = 1.209\frac{1}{N_H}\{(N_H - 1)\eta_{H_0} + \eta_{H_1}\} \quad (43)$$

where η_{H_1} is the collection efficiency of the Happel cell with one deposited particle. Combining Eqs. 43 and 33, one has

$$\eta_{u_1} - \eta_{u_0} = \frac{1.209}{N_H}(\eta_{H_1} - \eta_{H_0}). \quad (44)$$

If the UBE is assumed to have N_c capillaries and particle deposition occurs in the ith capillary, then the UBE collection efficiency, η_{u_1}, is

$$\eta_{u_1} = \frac{1}{Q_T}(q_1\eta_{1_0} + q_2\eta_{2_0} + \ldots + q_i\eta_{i_1} + \cdots + q_{N_c}\eta_{N_{c_0}}) \quad (45)$$

where η_{i_1} is the collection efficiency of the ith pore with one deposited particle. If one neglects the change in flow rate through all the pores due to the presence of one deposited particle in the ith pore, or

$$q_{j_0} = q_j \quad (j = 1, 2, \cdots, N_c), \quad (46)$$

then from Eqs. 34 and 45, the increase in collection efficiency of the UBE due to the deposition of one particle in the ith pore is

$$\eta_{u_1} - \eta_{u_0} = \frac{q_i}{Q_T}(\eta_{i_1} - \eta_{i_0}). \quad (47)$$

It may appear to be possible to obtain η_{i_1} by equating Eq. 47 with Eq. 44. In reality, the $\eta_{u_1} - \eta_{u_0}$ term of Eq. 44 gives the average effect of one deposited particle on the increase

in collection efficiency. The effect of one deposited particle in the ith capillary given by Eq. 47 may be either greater or less than the average value since the capillaries are not uniform in size. The average effect due to the deposition of one particle is

$$\frac{q_{10}\eta_{1_0}}{Q_T\eta_{u_0}}\left(q_1^{(1)}\eta_{1_1}+q_2^{(1)}\eta_{2_0}+q_3^{(1)}\eta_{3_0}+\cdots+q_{N_c}^{(1)}\eta_{N_{c_0}}\right)$$
$$+\frac{q_{20}\eta_{2_0}}{Q_T\eta_{u_0}}\left(q_1^{(2)}\eta_{1_0}+q_2^{(2)}\eta_{2_1}+q_3^{(2)}\eta_{3_0}+\cdots+q_{N_c}^{(2)}\eta_{N_{c_0}}\right)+\cdots$$
$$+\frac{q_{N_{c_0}}\eta_{N_{c_0}}}{Q_T\eta_{u_0}}\left(q_1^{(N_c)}\eta_{1_0}+q_2^{(N_c)}\eta_{2_0}+q_3^{(N_c)}\eta_{3_0}+\cdots+q_{N_c}^{(N_c)}\eta_{N_{c1}}\right)$$
$$=Q_T\eta_{u_1} \quad (48)$$

where $(q_{i_0}\eta_{i_0})/(Q_T\eta_{u_0})$ is the probability for one particle to be deposited in the ith capillary; and $q_i^{(k)}$ is the flow rate of the ith capillary when one particle is deposited in the kth capillary. If one neglects the flow rate change due to the deposited particle, then

$$q_i^{(1)}=q_i^{(2)}=\cdots=q_i^{(N_c)}=q_{i_0}=q_i \quad i=1,2,\ldots,N_c. \quad (49)$$

By substituting Eq. 34 into Eq. 48, the collection efficiency change of the UBE in terms of the cylindrical pore model can be expressed as

$$\eta_{u_1}-\eta_{u_0}=\frac{1}{Q_T^2\eta_{u_0}}\left\{q_1^2\eta_{1_0}(\eta_{1_1}-\eta_{1_0})+q_2^2\eta_{2_0}(\eta_{2_1}-\eta_{2_0})+\cdots\right.$$
$$\left.+q_{N_c}^2\eta_{N_{c_0}}^2\eta_{N_{c_0}}(\eta_{Nc_1}-\eta_{Nc_0})\right\}. \quad (50)$$

It is clear that $\eta_{i_1}-\eta_{i_0}$ cannot be found from $\eta_{u_1}-\eta_{u_0}$ without additional information. To circumvent this difficulty, as an approximation, one may assume that Eqs. 42 and 47 are equivalent. Then the change in collection efficiency of the ith pore due to one deposited particle can be expressed as

$$\eta_{i_1}-\eta_{i_0}=\frac{Q_T}{q_i}\frac{1.209}{N_H}(\eta_{H_1}-\eta_{H_0}). \quad (51)$$

The preceding expression gives the increase in the collection efficiency of a capillary due to one deposited particle. Since the results shown in Figure 8 (or Eq. 41) indicate that the change in collection efficiency is approximately a linear function of the contributions of all deposited particles, Eq. 51 may be generalized to give the difference between the collection efficiency with $(p+1)$ deposited particles and that with p deposited particles, or

$$(\Delta\eta)_i=\eta_{i_{p+1}}-\eta_{i_p}=\frac{Q_T}{q_i}\frac{1.209}{N_H}(\eta_{H_{p+1}}-\eta_{H_p})$$
$$=\frac{Q_T}{q_i}\frac{1.209}{N_H}\eta_{H_0}B. \quad (52)$$

Equation 52 can be used to estimate the change in the collection efficiency of any pore in a UBE due to the deposition of one additional particle.

Collection efficiency during the third stage of particle deposition

During the third stage of deposition, the collection efficiency is unity since all the particles associated with the liquid flow through a pore are retained at the pore inlet to form a deposit (or cake). The third stage of deposition is operative if the interstitial velocity is not excessively large and does not exceed the critical velocity.

Critical velocity

Deposition requires the adhesion of impacting particles on the collector surface. If the liquid velocity in the capillary is excessively large, a correspondingly large drag force acting on impacting particles may prevent their deposition. It may be argued that there exists a critical velocity, v_c, beyond which particle deposition becomes impossible. In principle, one may estimate v_c by relating the tangential force acting on a particle at a distance of one particle radius away from the surface of the deposit layer or a collector to the net normal force multiplied by the friction coefficient. The tangential drag force acting on a particle, F_θ, may be approximated as (Goldman et al., 1967)

$$F_\theta=1.7005^*6\pi\mu a_p v_\theta \quad (53)$$

where v_θ is the tangential velocity at a distance a_p from the surface of the deposit layer or a collector.

When a particle is sufficiently close to the surface of a collector, the London force, F_{Lon}, becomes the dominant force along the normal direction. This force is given as

$$F_{\text{Lon}}=\frac{Ha_p}{6z_0^2} \quad (54)$$

where H is the Hamaker constant and z_0 is the distance of minimum separation. According to Herzig et al. (1970), z_0 is given as

$$z_0^2=\frac{2H}{\pi a_p^2 g(\rho_p-\rho_w)} \quad (55)$$

where g is the gravity and ρ_p and ρ_w are particle density and fluid density, respectively. Thus one can determine the critical velocity by equating Eq. 53 to Eq. 54 and the value of the friction coefficient. In practice, the critical velocity is often determined experimentally, and the preceding approach is used mostly as a guide and qualitative analysis. Rege and Fogler (1988) suggested the use of $v_c=0.08$ cm/s, while Mackie et al. proposed a value of 2 cm/s. Clearly, this critical velocity varies with the condition of the experiment and may be selected as a best fitting value with experiment.

Since the deposit formed over a capillary inlet is nonuniform, the local interstitial velocity decreases with the decrease of the deposit layer thickness. If the fluid velocity at a

distance of one particle radius away from the pore surface in the last segment of a capillary pore (the MNth segment of Figure 5) exceeds the critical velocity value, then the collection efficiency of the capillary reduces to zero.

Simulation Procedure

Initialization

Initially, the filter height, L, and the number of capillaries present in a unit-bed element, M are specified. (The cross-sectional area of the UBE, S, may be obtained by $S = [4/\pi\epsilon_0(1 - S_{wi})] \sum_{i=1}^{M} (d_i)^2$, where d_i is the diameter of the ith capillary.) The number of the unit bed elements, N, is determined from Eq. 2 with N being the integer closest to L/l.

The size of each of the M pores can be determined from the number of pores present in a UBE, M, and the pore-size distribution data. This pore distribution is the same for all the UBEs.

Once the pore sizes are known, the initial hydraulic conductivity (or initial pressure drop), flow rate, and collection efficiency can be determined from Eqs. 14, 8, and 37.

Simulation

Assume that the states of every pore of the UBEs are known at a given time. The state of a pore is defined by the number of deposited particles present in the pore $(N_p)_{ij}$, which, in turn, defines its hydraulic conductivity, collection efficiency, and the geometry (the shape of the deposit layer). Simulation will be made according to the following steps:

(1) Particles are introduced into the filter one at a time.

(2) If a particle arrives at a particular UBE, it may enter any one of the pores of the UBE. The probability of the particle's entering a given pore is proportional to the fluid flow rate through that pore. A random number between zero and unity (*RAN* A) is generated. If *RAN A* is

$$\frac{1}{(Q_T)_j} \sum_{k=1}^{i-1} q_{kj} \le \text{RAN A} \le \frac{1}{(Q_T)_j} \sum_{k=1}^{i} q_{kj}, \qquad (56)$$

then the ith pore is the pore into which the particle enters.

(3) To determine whether or not the particle is captured, we note that the collection efficiency may be interpreted as the probability of a given entering particle being collected. By generating another random number (*RAN B*), if *RAN B* is less than the collection efficiency of the ith pore, the particle is assumed to be deposited.

(4) If the particle escapes collection, it goes to the next UBE. Repeat step 2 and step 3 until the particle either becomes deposited or escapes. If the particle is not captured by the filter bed, go to step 1.

(5) If the particle is captured by the ith pore of the jth UBE, the value of $(N_p)_{ij}$ is increased by one. With the new value of $(N_p)_{ij}$, $(R_d)_{ij}$ can be obtained from Eq. 13. Based on the new deposit layer profile, calculate the fluid velocity at a distance of one particle radius away from the deposit layer in the last segment of the jth pore.

(6) Update the collection efficiency of the pore based on the new value of $(N_p)_{ij}$. Specifically,

(*a*) $\eta_{ij} = 0$, if the fluid velocity > critical velocity;

(*b*) Equation 52, if $(R_d)_{ij} > 3a_p$ (or $7a_p$);

(*c*) $\eta_{ij} = 1$, $(R_d)_{ij} < 3a_p$(or $7a_p$).

(7) The hydraulic conductivity of a pore changes as the number of deposited particles increases. However, since the effect due to the deposition of one particle is usually rather small, in order to reduce the simulation time, the hydraulic conductivity of the pores present in all the UBEs is calculated once for every 50 particles injected. The number of 50 was found satisfactory by trial and error. The value of α_{ij} is determined according to

(*a*) Equation 18, if $(R_0)_{ij} - (R_d)_{ij} \le d_p$;

(*b*) Equation 28, if $(R_d)_{ij} > 3a_p$(or $7a_p$);

(*c*) Equation 29, if $(R_d)_{ij} < 3a_p$(or $7a_p$).

(8) Repeat steps 1 through 7 until all the particles are injected into the model system.

A description of the simulation algorithm is shown in Figure 9.

Simulation Results

A number of sample simulations were made as part of this study and some of the results are presented here. The conditions used for simulation are given in Table 1. Note that they are the same as those used by Chiang (1985a) before. The capillary size distribution is obtained from the pore-constriction distribution data of Payatakes (1974) (Figure 10) using the procedure described earlier and shown in Figure 11. Payatakes' data were obtained from a medium composed of grains (glass sphere) of diameter 470 μm, while in this simulation, the grain diameter is assumed to be 505 μm.

As described before, the simulation algorithm gives the number of deposited particles for each capillary, $(N_p)_{ij}$, and its hydraulic conductivity α_{ij}, $i = 1, \ldots, M$ and $j = 1, \ldots, N$ as a function of the number of the particle injected, n_{in}. In deep-bed filtration, filter performance is characterized by the effluent concentration and media permeability (or the pressure drop required to maintain a given flow rate) histories. The relationship between n_{in} and time, t, is simply

$$n_{in} = (u_s)(S)c_{in}t \text{ or } t = n_{in}/(u_s S c_{in}) \qquad (57)$$

where u_s is the superficial velocity, S is the cross-sectional area of the unit-bed element, and c_{in} is the particle number concentration of the influent.

The change in permeability (or pressure drop) can be found from Eqs. 10 and 11. The profile of the particle concentration of the suspension is

$$\frac{c_{\text{eff}}}{c_{in}} = \frac{n_{in} - \sum_{j=1}^{z/l} \sum_{i=1}^{M} (N_p)_{ij}}{n_{in}} \qquad (58)$$

where z is the coordinate along the direction of the flow with its origin at the inlet.

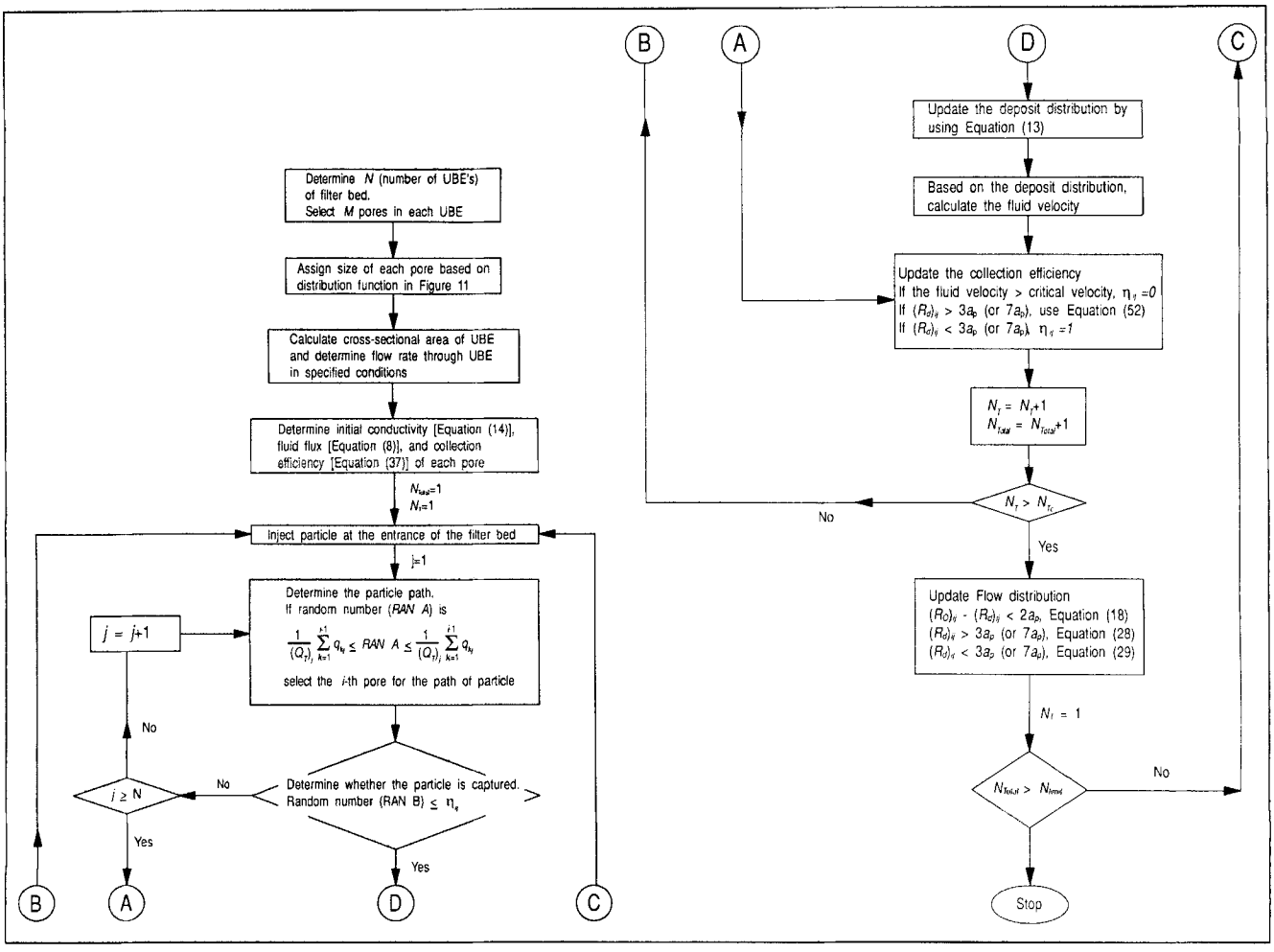

Figure 9. Simulation algorithm for the prediction of permeability reduction.

Table 1. Experimental and Simulation Conditions for Model Predictions and Comparisons

Experimental Conditions						
Exp.	η_0 (Exp.)	d_F (μ)	d_g (μ)	μ_s (cm/s)	C_{in} (ppm)	N_R
Chiang						
Run no. 1	2.820×10^{-2}	26	505	0.1	9	0.0515
Run no. 2	2.430×10^{-2}	26	505	0.2	5	0.0515
Run no. 5	1.587×10^{-2}	19.5	505	0.1	12	0.0385

Simulation Conditions	
N (no. of UBE's)	10 (L = 0.5 cm)
M (no. of pores in a UBE)	100
MN (no. of segments in Figures 6 & 7)	20
S_{wi} (irreducible saturation)	0.111
ϵ_0 (initial bed porosity)	0.41
Cross-sectional area of a UBE	0.231 (cm^2)
Flow rate through a UBE	
Chiang's run nos. 1 and 5	0.023 (cm^3/s)
Chiang's run no. 2	0.046 (cm^3/s)
B (constant in Eq. 42)	
Chiang's run nos. 1 and 2	1.809E-4
Chiang's run no. 5	7.365E-5

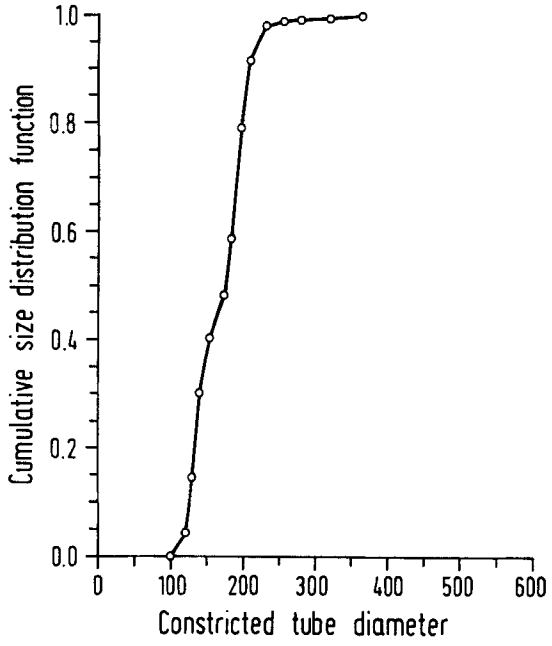

Figure 10. Constricted-tube-size distribution (Payatakes, 1973).

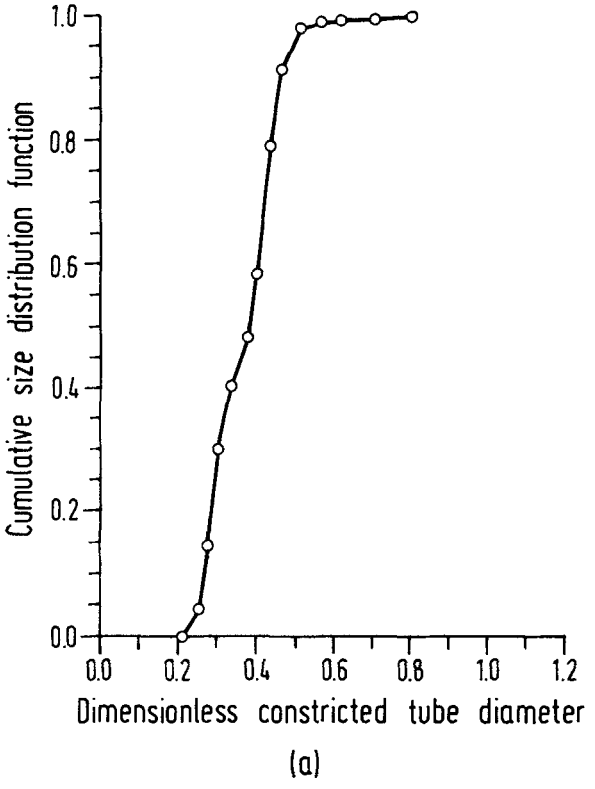

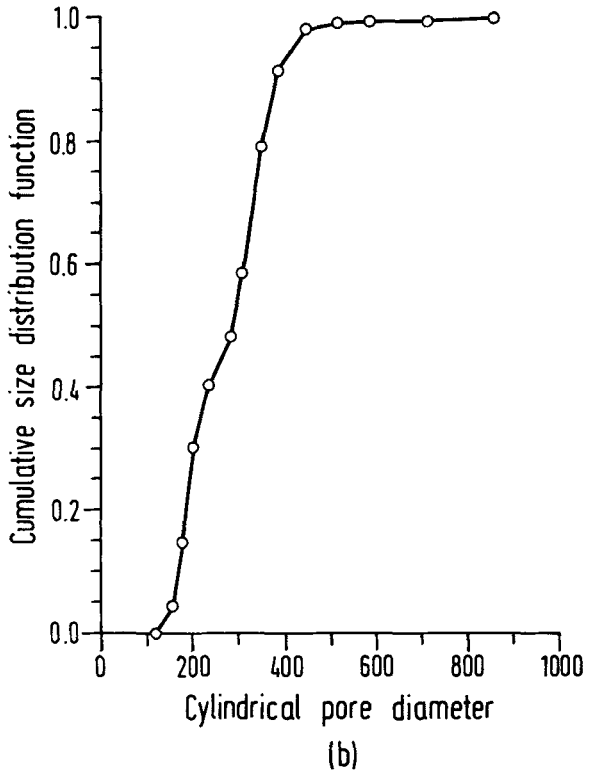

Figure 11. Distribution of the constricted-tube diameter and its corresponding distribution of the cylindrical-pore diameter.

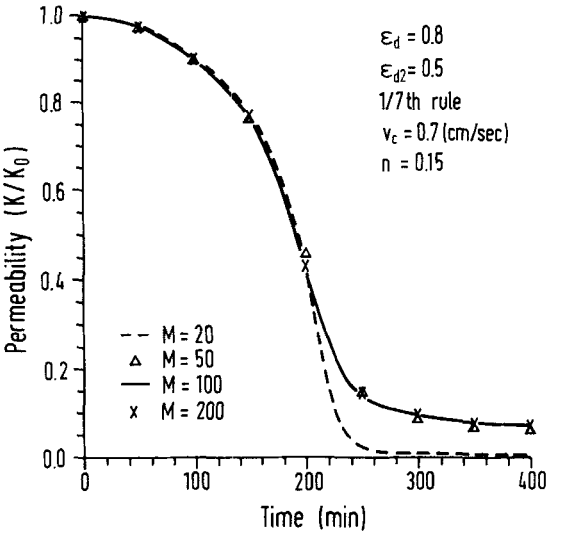

Figure 12. Effect of the number of pores in a UBE on permeability reduction.

Statistical nature of the simulation results

In this simulation, particle deposition is considered as a stochastic process. Accordingly, a number of simulations must be made in order to obtain the average behavior. Further, it is also necessary to consider a sufficiently large number of capillaries so that the simulation results are independent of the value of M used. The effect of the number of capillaries used in a simulation on the simulation results is shown in Figure 12. In Figure 12, the reduction of the overall permeability (K/K_0) as a function of time for a particular case obtained from simulations using $M = 20$, 50, 100, and 200 is shown. It is clear that the results were essentially the same if M were greater than 50. A smaller value of M tends to over-

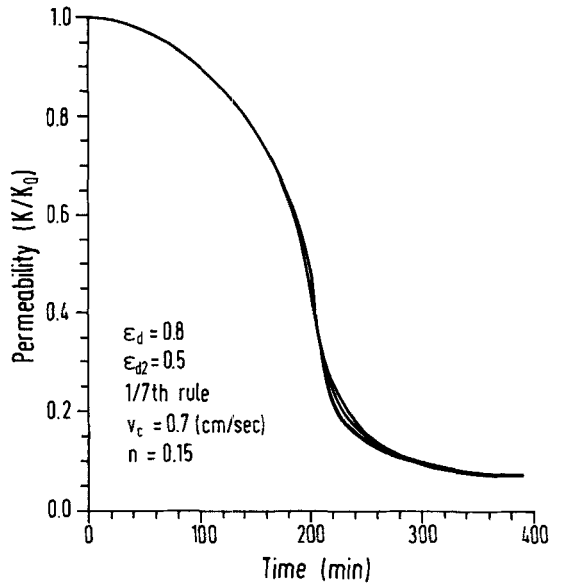

Figure 13. Simulation of permeability from eight independent runs under the same condition.

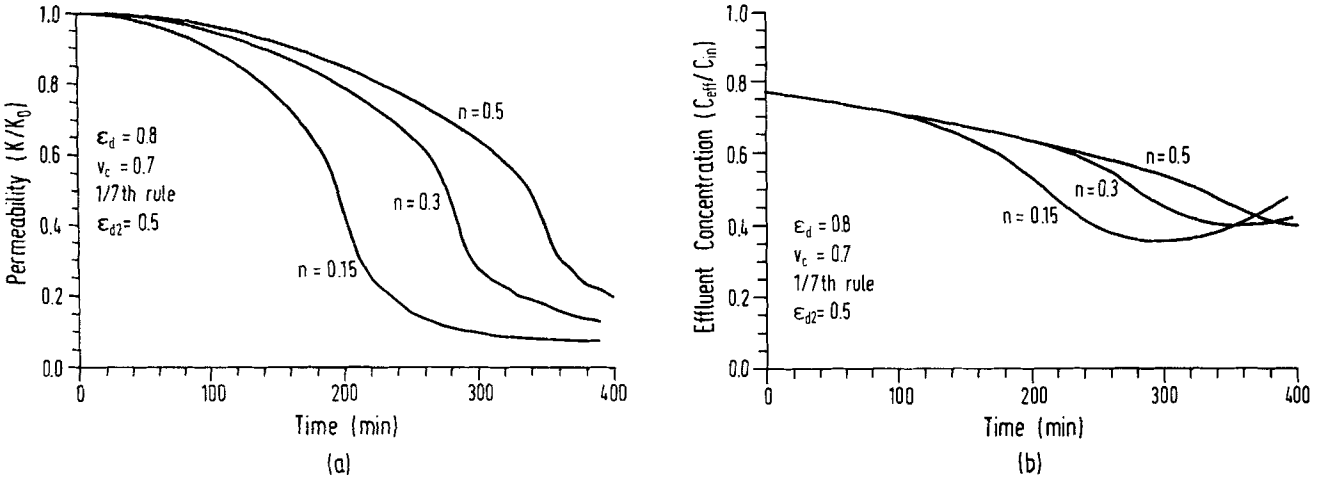

Figure 14. Effect of deposit distribution (n) in the pore on permeability reduction and effluent concentration under conditions of Run No. 2 of Chiang (1983).

predict the change in permeability in the later stages of deposition.

The variability of the permeability reduction obtained in different simulations is shown in Figure 13, which gives the results for eight independent simulation runs (with different seed numbers for random number generations). The results are indeed different, but the differences are rather insignificant. All the results reported in this section were obtained using $M = 100$ and the average of eight independent runs.

Effect of model parameters

A parametric study was made to examine the effects of the various model parameters. The results are as follows:

Effect of Deposit Distribution. The effect of the deposit distribution is shown in Figure 14. As expected, a larger value of n (see Eq. 12a) gives a slower permeability reduction since pore blocking is delayed if the deposits are more uniform. The effect of deposit nonuniformity on filtrate quality, however, is more complex. Initially, a more rapid pore blocking enhances particle deposition and therefore the filtrate quality. As pore blocking becomes more pronounced, however, the local interstitial velocity increases and may exceed the critical velocity, and part of the filter becomes nonretentive. This behavior is shown by an initial improvement in filtrate quality followed by its deterioration, as shown in Figure 14b.

Effect of the Porosity of a Deposit Layer Formed by the Blocking Mode of Deposition. If the porosity of the deposit layer at the inlet of a capillary pore is high, then the resistance to fluid flow through the pore will be low, leading to a low permeability reduction. This behavior is shown in Figure 15a. The extent of permeability reduction is reduced with the increase of ϵ_{d_2}. The increase in ϵ_{d_2} also favors the improvement of filtrate quality. A higher value of ϵ_{d_2} means more fluid flow through pores covered with internal cakes. When ϵ_{d_2} is sufficiently high, fluid redistribution from blocked to open pores becomes less. As a result, it is less likely that the interstitial velocity of certain pores exceeds the critical veloc-

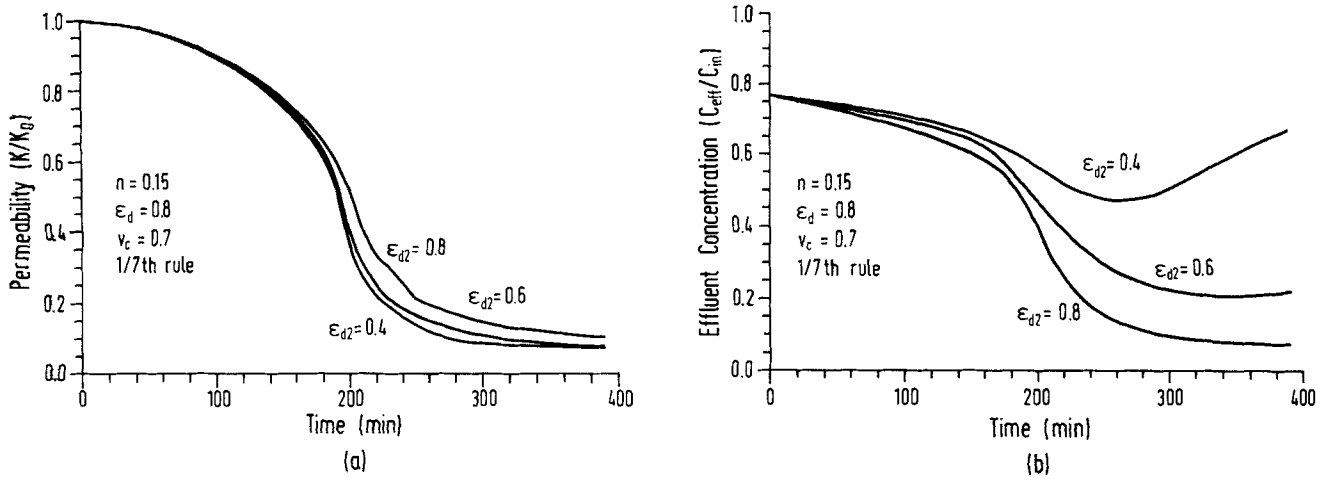

Figure 15. Effect of the porosity of the deposit formed by pore blocking on permeability reduction and effluent concentration under conditions of Run No. 2 of Chiang (1983).

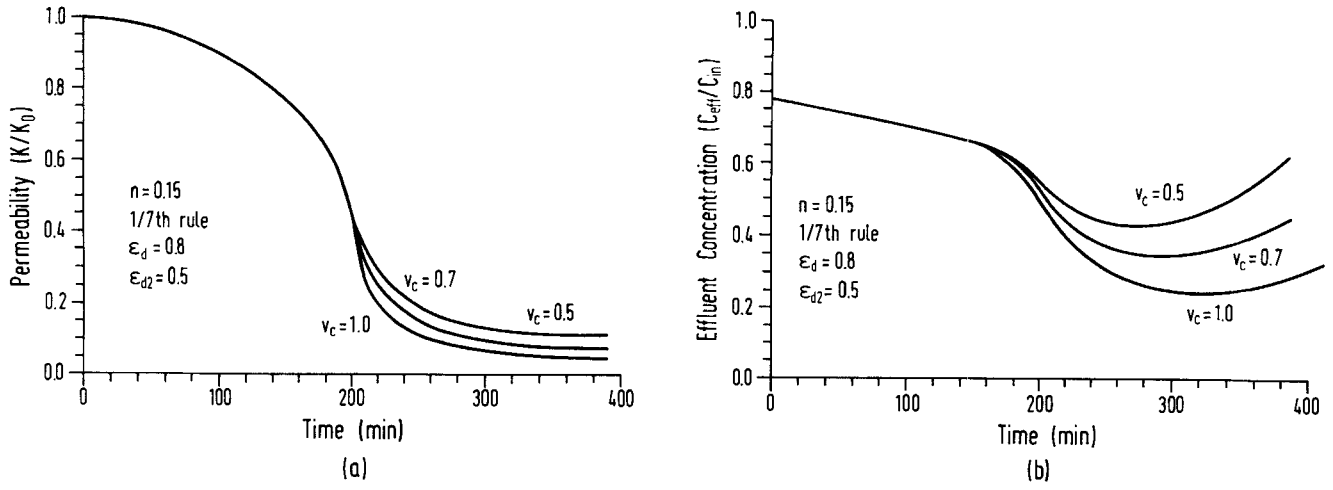

Figure 16. Effect of the critical velocity on permeability reduction and effluent concentration under conditions of Run No. 2 of Chiang (1983).

ity. Thus, for the case $\epsilon_{d_2} = 0.8$, the effluent concentration decreases monotonically and approaches a certain constant value. In contrast, for a lower value of ϵ_{d_2}, the effluent concentration may first decrease and then increase with time.

Effect of the Critical Velocity. The effect of the critical velocity on permeability reduction and effluent quality is shown in Figure 16. Since a small critical velocity value implies that a filter becomes nonretentive sooner, a lesser permeability reduction and an earlier filtrate quality deterioration may be expected. The results shown in Figure 16 are consistent with this argument.

Effect of the pore-blocking criterion. The effect of the pore-blocking criterion is shown in Figure 17 for a particular case with $n = 0.15$. Similar to Figure 16, early pore blocking or the use of the seventh rule instead of the third rule in simulation leads to a more rapid permeability reduction. Furthermore, since blocked pores provide more efficient filtration (at least initially), the improvement in filtrate quality is more pronounced with the use of the seventh rule than the fifth (or third) rule. On the other hand, with more complete blocking occurring, earlier deterioration in filtrate quality can be expected when the seventh rule is used.

Comparison with Experiment

The experimental data used to compare with model predictions were obtained by Chiang (1983). The experimental conditions are similar to those used in the simulation (see Table 1).

As stated before, the permeability reduction model has a number of parameters, some of which cannot be determined independently. In fact, these parameters are adjustable parameters and can be determined by comparisons between predictions and experiments. On the other hand, for a model such as the one on permeability reduction to be useful, all the model parameters must be known beforehand. In the fol-

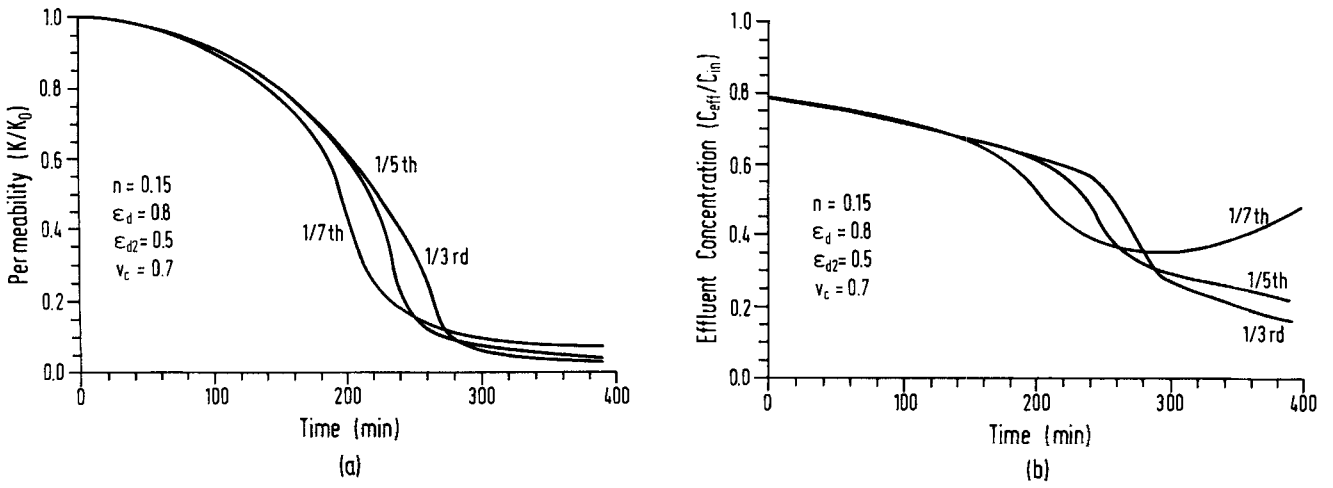

Figure 17. Effect of the pore-blocking criterion on permeability reduction and effluent concentration under conditions of Run No. 2 of Chiang (1983).

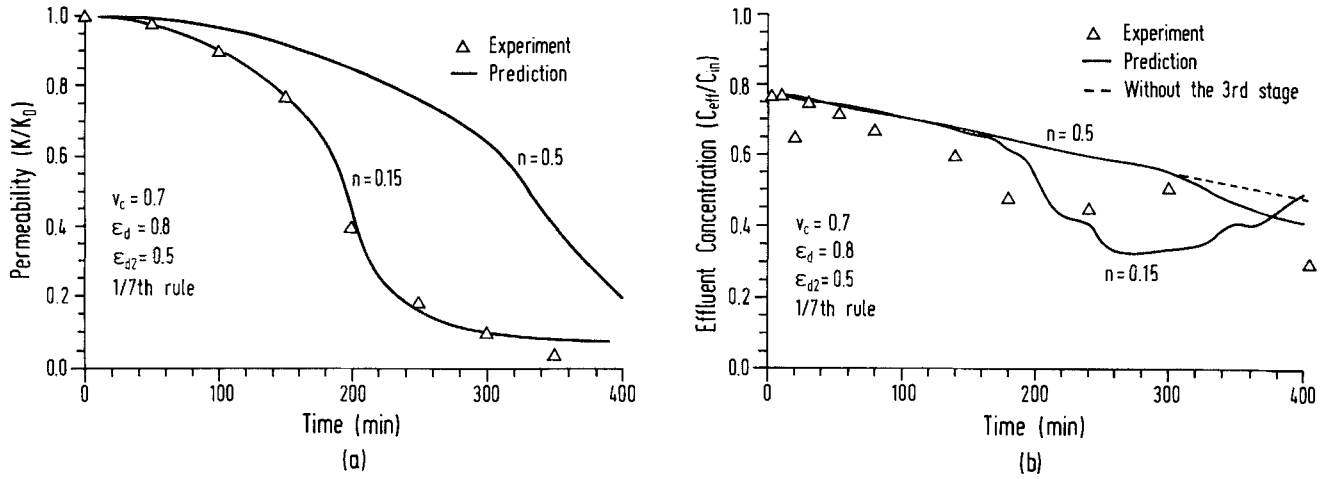

Figure 18. Histories of permeability reduction and effluent concentration between model predictions and results of Run No. 2 of Chiang (1983).

lowing paragraphs, we first discuss the estimation of the various model parameters.

Among the parameters, the initial medium porosity (ϵ_0) can be readily determined. For a granular bed, ϵ_0 covers a fairly narrow range (0.35–0.45). The porosity of the deposit over the pore surface can be estimated from the simulation results of Jung (1991) and assumed to be 0.8, as previously stated. Assuming that the Carman-Kozeny equation is applicable, k_m and k_d can be readily determined.

The porosity of the deposit layer formed at the pore inlet is one of the parameters that cannot be determined independently. Since the deposit is formed by straining, the deposit may be viewed as similar to a filter cake, and a porosity on the order of 0.5 may be assumed. For the other parameters, the following values are assigned:

(1) The critical velocity is selected to be 0.7 cm/s.

(2) The seventh rule is used for the onset of pore blocking.

(3) The value of n of Eq. 12a is taken to be either 0.15 or 0.5.

The abovementioned values (with $n = 0.15$) were selected on the basis that predictions based on these values gave good agreement with experiments for Run No. 2 reported by Chiang. Prediction based on $n = 0.5$ was made since there does not appear to be any rational basis for selecting n.

The comparisons between prediction and experiment at Chiang's Run No. 2 are shown in Figure 18. The agreement is excellent for permeability reduction. The filtrate quality results are somewhat less satisfactory, mainly because of the relatively large data scattering. Also included in Figure 18b are predictions with the absence of the third stage of deposition. With pore blocking, filtrate quality improvement takes place more slowly but monotonically.

To assess the predictive capability of the model, predicted histories of permeability and filtrate quality corresponding to the conditions of Chiang's Run No. 1 and the experimental results are shown in Figure 19. The agreement is less satisfac-

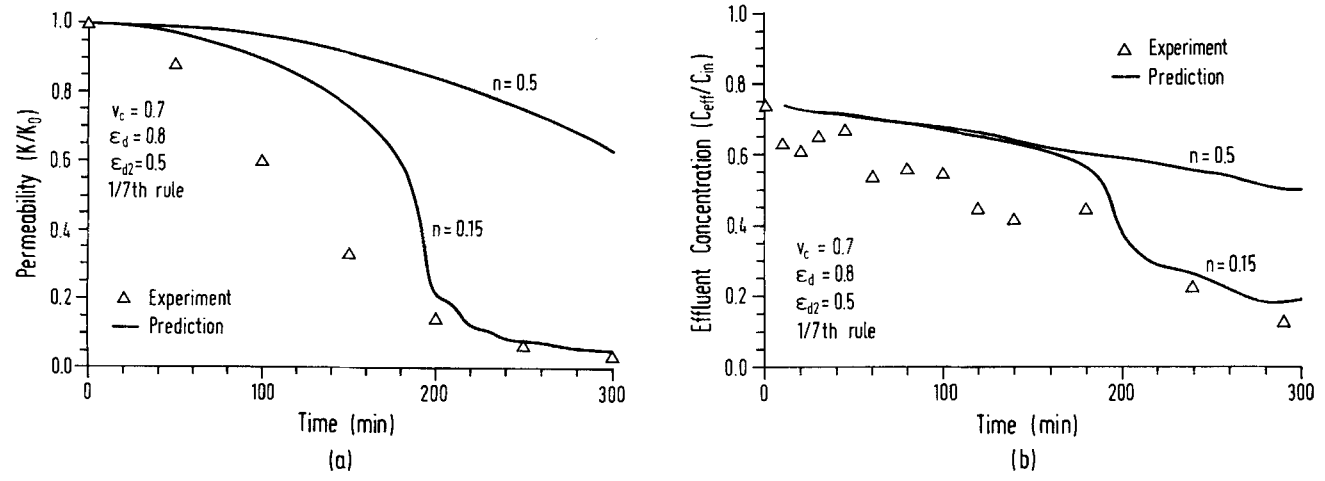

Figure 19. Histories of permeability reduction and effluent concentration between model predictions and results of Run No. 1 of Chiang (1983).

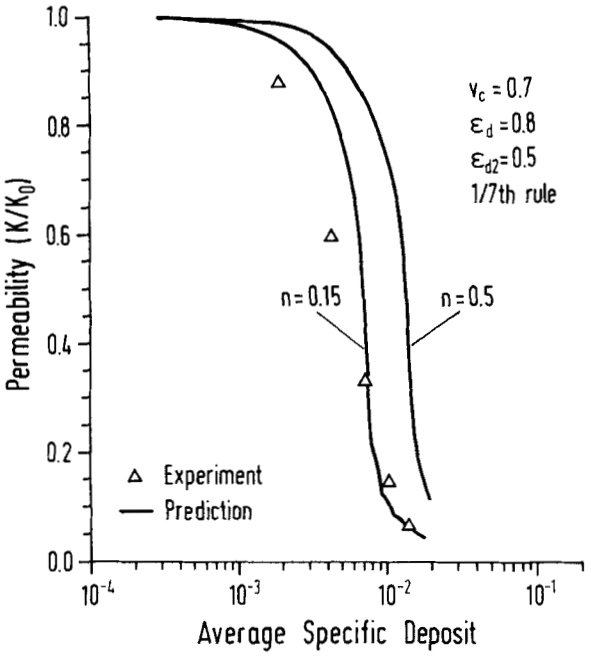

Figure 20. Permeability reduction vs. average specific deposit in a filter bed between model predictions and results of Run No. 1 of Chiang (1983).

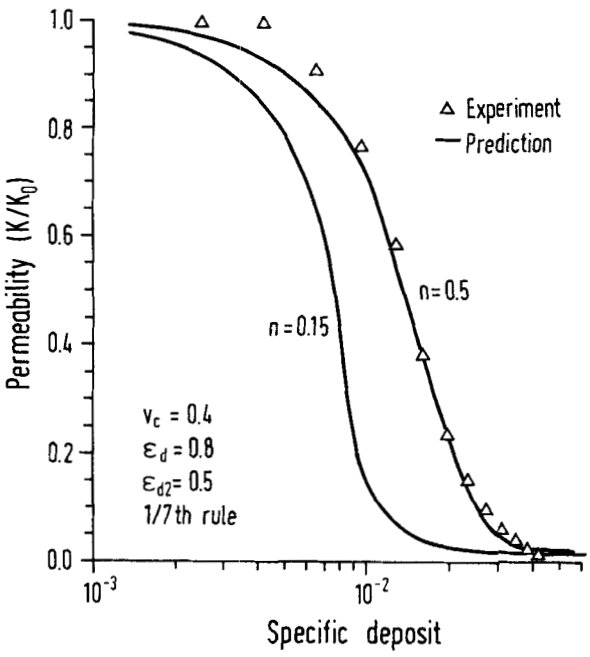

Figure 22. Permeability reduction vs. average specific deposit in a filter bed between model predictions and results of Run No. 5 of Chiang (1983).

tory if $n = 0.15$ is used. This poor agreement arises largely from underestimating the rate of filtration (or overestimating the effluent concentration). This situation can be observed by comparing the predicted permeability reduction with the extent of deposition (this prediction can be made by combining Figures 19a and 19b with experiments). The agreement was indeed good, as shown in Figure 20.

Another comparison between predictions and experiment is given in Figures 21 and 22. The parameter values used are the same as before except that the critical velocity is changed to account for the difference in particle size. As shown previously, v_c can be expected to be

$$v_c = 0.7\,(19.5/26)^2 = 0.4\ (\mathrm{cm/s}).$$

On the whole, the agreement between prediction and Run No. 5 of Chiang's experiment was very good, especially if $n = 0.5$, as shown in Figure 21.

These three sets of comparisons demonstrate that the permeability reduction model can indeed be applied as a predictive tool, in spite of the rather large number of parameters present in the model. With the exception of one parameter (i.e., n), all the parameters can be either determined independently or assigned constant values. Even for the pa-

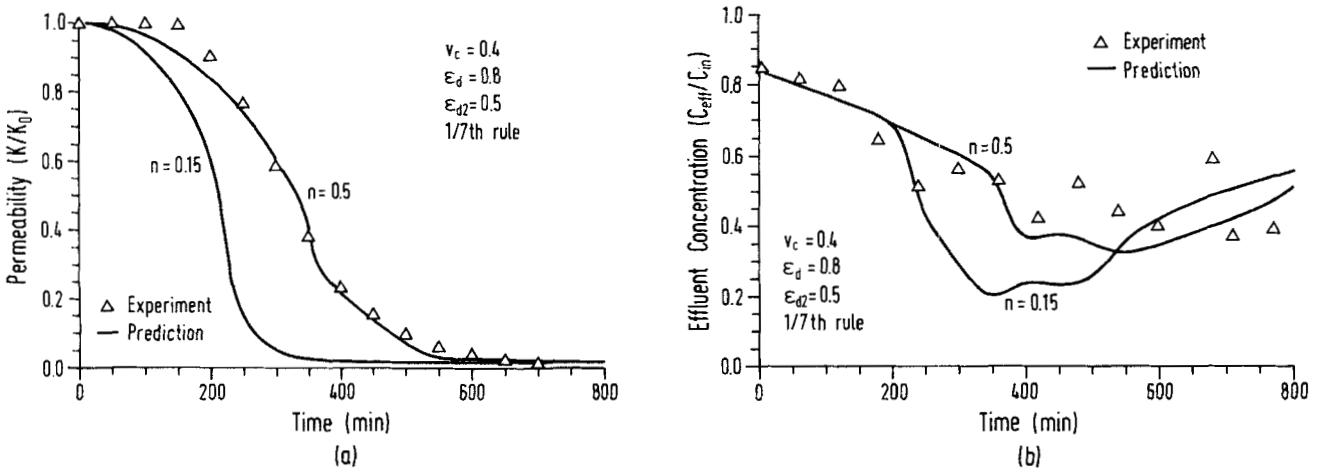

Figure 21. Histories of permeability reduction and effluent concentration between model predictions and results of Run No. 5 of Chiang (1983).

rameter n, whose value cannot be known *a priori*, predictions nevertheless can be made by using several n values over a fairly narrow range in order to obtain some estimates for permeability reduction. Such prediction capability was not available prior to the present work.

Notation

A_s = Happel parameter defined as $2(1-h^5)/w$
$h = (1-\epsilon)^{1/3}$
N_G = gravitational parameter defined as $[2a_p^2(\rho_p - \rho_f)g]/[9\pi\mu u_s]$
N_{Lo} = London force parameter defined as $H/[9\pi\mu a_p^2 u_s]$
N_{Pe} = Peclet number defined as $u_s a_g/D_{BM}$, where D_{BM} is the Brownian diffusivity
N_R = interception parameter defined as d_p/d_g when d_p and d_g are the particle diameter and grain diameter, respectively
$w = 2-3h+3h^5-2h^6$

Literature Cited

Chiang, H. W., "Transient Behavior of Deep Bed Filtration," PhD Diss., Syracuse Univ., Syracuse, NY (1983).

Chiang, H. W., and C. Tien, "Dynamics of Deep Bed Filtration: I. Analysis of Two Limiting Situations," *AIChE J.*, **31**, 1349 (1985a).

Chiang, H., W., and C. Tien, "Dynamics of Deep Bed Filtration: II. Experiment," *AIChE J.*, **31**, 1360 (1985b).

Choo, C.-U., "A Model for Clogged Filter Media," PhD Diss., Syracuse Univ., Syracuse, NY (1993).

Fatt, I., "The Network Model of Porous Media," Pet. *Trans AIME*, **207**, 144 (1956).'

Goldman, A. J., R. G. Cox, and H. Brenner, "Slow Viscous Motion of a Sphere Parallel to a Plane Wall," *Chem. Eng. Sci.*, **22**, 637 (1967).

Happel, J., and H. Brenner, *Low Reynolds Number Hydrodynamics*, Prentice-Hall, Englewood Cliffs, NJ (1965).

Herzig, J. P., D. M. Leclerc, and P. L. Goff, "Flow of Suspensions through Porous Media—Application to Deep Filtration," *Ind. Eng. Chem.*, **62**(5), 8 (1970).

Imdakm, A. O., and M. Sahimi, "Transport of Large Particles in Flow through Porous Media," *Phys. Rev. A*, **36**, 5304 (1987).

Imdakm, A. O., and M. Sahimi, "Computer Simulation of Particle Transport Processes in Flow through Porous Media," *Chem. Eng. Sci.*, **46**, 1977 (1991).

Jung, Y., "Granular Filtration of Mono-Dispersed and Polydispersed Aerosols," PhD Diss., Syracuse Univ., Syracuse, NY (1991).

Mackie, R. I., R. M. W. Horner, and R. J. Jarvis, "Dynamic Modeling of Deep Bed Filtration," *AIChE J.*, **33**, 1761 (1987).

O'Melia, C. R., and W. Ali, "The Role of Retained Particles in Deep Bed Filtration," *Prog. Water Technol.*, **10**, 167 (1978).

Payatakes, A. C., "A New Model for Granular Porous Media—Application to Filtration through Packed Beds," PhD Diss., Syracuse Univ., Syracuse, NY (1973).

Payatakes, A. C., R. Rajagopalan, and C. Tien, "Application of Porous Media Models to the Study of Deep Bed Filtration," *Can. J. Chem. Eng.*, **52**, 722 (1974).

Rajagopalan, R., and C. Tien, "Trajectory Analysis of Deep Bed Filtration with the Sphere-in-Cell Porous Media Model," *AIChE J.*, **22**, 523 (1976).

Rajagopalan, R., and C. Tien, "Single Collector Analysis of Collection Mechanisms in Water Filtration," *Can. J. Chem. Eng.*, **55**, 246 (1977).

Rege, S. D., and H. S. Fogler, "Network Model for Straining Dominated Particle Entrapment in Porous Media," *Chem. Eng. Sci.*, **42**, 1553 (1987).

Rege, S. D., and H. S. Fogler, "A Network Model for Deep Bed Filtration of Solid Particles and Emulsion Drops," *AIChE J.*, **34**, 1761 (1988).

Spielman, L. A., and J. A. FitzPatrick, "Theory for Particle Collection under London and Gravity Forces," *J. Colloid Inter. Sci.*, **42**, 607 (1973).

Tien, C., *Granular Filtration of Aerosols and Hydrosols*, Butterworths-Heinemann, Boston (1989).

Tien, C., R. M. Turian, and H. Pense, "Simulation of the Dynamic Behavior of Deep Bed Filters," *AIChE J.*, **25**, 385 (1979).

Todd, A. C., J. E. Somerville, and G. Scott, "The Application of Depth of Formation Damage Measurements in Predicting Water Injectivity Decline," *SPE 12498* Feb. (1984).

Vaidyanathan, R., and C. Tien, "Hydrosol Deposition in Granular Beds," *Chem. Eng. Sci.*, **43**, 289 (1988).

Vaidyanathan, R., and C. Tien, "Hydrosol Deposition in Granular Media under Unfavorable Condition," *Chem. Eng. Sci.*, **46**, 967 (1991).

Vigneswaran, S., and C. Tien, "Transient Behavior of Deep-Bed Filtration of Brownian Particles," *Chem. Eng. Sci.*, **42**, 2729 (1987).

Vigneswaran, S., and R. K. Tulachan, "Mathematical Modelling of Transient Behavior of Deep Bed Filtration," *Water Res.*, **22**, 1093 (1988).

Yao, K.-M., M. T. Habibian, and C. R. O'Melia, "Water and Waste Water Filtration: Concepts and Applications," *Environ. Sci. Technol.*, **5**, 1105 (1971).

Manuscript received Aug. 16, 1993, and revision received July 18, 1994.